Indonesian Journal of Environmental Management and Sustainability
e-ISSN:2598-6279 *p*-ISSN:2598-6260

IJEMS

Research Paper

Hydrochar Derived from *Pennisetum setaceum* for Congo Red Adsorption: A Low-Cost Bioadsorbent from Invasive Grass

Icha Aulia Karvenia[1], Idha Royani[1], Risfidian Mohadi[1*]

[1] *Master Program of Materials Science, Graduate School, Universitas Sriwijaya, Palembang, 30139, Indonesia*
***Corresponding author e-mail**: risfidian.mohadi@unsri.ac.id

Abstract
This study investigates the adsorption performance of hydrochar derived from *Pennisetum setaceum* (PS) through hydrothermal treatment at 250°C for various reaction times (1-4 hours) for the removal of Congo Red (CR) dye from aqueous solutions. The materials were characterized using FTIR, XRD, SEM–EDS, BET, and pH_{pzc} analysis to evaluate changes in functional groups, crystallinity, morphology, elemental composition, and surface charge. FTIR spectra confirmed the presence of oxygen-containing functional groups (O−H, C=O, C−O−C, C−O), while XRD patterns indicated a transition from amorphous to partially crystalline structures, followed by re-amorphization at longer reaction times. SEM images revealed a progressive increase in porosity and surface roughness, accompanied by an increase in carbon content, as shown by EDS. BET analysis of HPS-4 further confirmed its mesoporous structure with a surface area of 9.316 m^2/g, which supports enhanced adsorption performance. Adsorption experiments demonstrated that the optimum pH for CR removal by HPS-4 was 5, with a maximum capacity of 51.674 ± 5.468 mg/g. Kinetic studies followed the pseudo-first-order model, and equilibrium data fitted well with the Langmuir isotherm, indicating monolayer adsorption. Thermodynamic analysis showed the process was spontaneous and exothermic ($\Delta H^\circ = -44.07$ kJ/mol). The proposed adsorption mechanism involves a combination of electrostatic attraction, hydrogen bonding, and π–π interactions between CR molecules and the aromatic structure of hydrochar. However, regeneration tests indicated a significant decrease in efficiency after the third cycle. These findings suggest that hydrochar from *Pennisetum setaceum* is a promising adsorbent for anionic dye removal, with optimal performance achieved under controlled hydrothermal conditions.

Keywords
Hydrochar, *Pennisetum setaceum*, Adsorption, Congo Red

Received: 18 May 2025, Accepted: 21 August 2025
https://doi.org/10.26554/ijems.2025.9.3.156-170

1. INTRODUCTION

Environmental pollution due to industrial wastewater, especially that containing synthetic dyes, is becoming an increasingly urgent issue to be addressed (Alegbe and Uthman, 2024; Kumari, 2024; Wibiyan et al., 2024; Wijaya and Yuliasari, 2023). One of the dyes often found in textiles, batik, and paper industry waste is Congo red, a type of azo dye that is anionic, toxic, difficult to biodegrade, and has the potential to cause health problems (Ahmad et al., 2024; Cui et al., 2025; He et al., 2025; Rianjanu et al., 2025). The presence of Congo red in water, even at low concentrations, can inhibit light penetration, disrupt the photosynthesis of aquatic organisms, and pose a risk to ecosystems and human health (Ahmad et al., 2023; He et al., 2025; Siddiqui et al., 2023). Therefore, the development of effective, economical, and environmentally friendly methods of handling the effluent is an urgent need.

Various techniques have been applied to remove dyes from wastewater, such as photocatalysis (da Silva et al., 2024; Farjadfar et al., 2022; Fattahimoghaddam et al., 2021), coagulation (Ahmed et al., 2022; Tolkou et al., 2025; Wei et al., 2022), membrane filtration (Dehingia et al., 2024; Kazak et al., 2023; Mortezapour et al., 2025), and adsorption (Jefri et al., 2024; Munonde et al., 2025; Siregar et al., 2021). Among these methods, adsorption is one of the most promising techniques due to its ease of implementation, high efficiency, and no harmful by-products (Badaruddin et al., 2022; Satyam and Patra, 2024; You et al., 2021). Nevertheless, the key challenge lies in identifying adsorbents that are not only highly effective but also cost-efficient and widely available (Akhtar et al., 2024; Badran et al., 2023; Dehghani et al., 2023). Various types of adsorbents have been utilized for this purpose, such as layered double

hydroxides (LDHs) (Jefri et al., 2025), zeolites (Bezerra et al., 2019), bentonites (Bessaha et al., 2023), and carbon-based materials (Phan et al., 2022). Among them, carbon-based materials are particularly favored due to their low cost, environmental friendliness, and abundance (Mohadi et al., 2022). One such material that has gained increasing attention is hydrochar.

Hydrochar is a carbonaceous solid material produced through hydrothermal carbonization (HTC) of wet biomass under moderate temperatures (typically 180–250°C) and self-generated pressure (Khanzada et al., 2024; Li et al., 2021; Ojewumi and Chen, 2024). Hydrochar has the advantages of a developed pore structure, the presence of active functional groups such as −OH and −COOH, and good thermal stability (Adawiyah et al., 2024; Kohzadi et al., 2023). Biomass rich in lignocellulose, such as agricultural waste, forestry residues, and wild grasses, is particularly suitable for hydrochar production because its complex structure of cellulose, hemicellulose, and lignin can be effectively converted into stable carbon frameworks (Cui et al., 2024; Güleç et al., 2021). These lignocellulosic precursors not only enhance the structural integrity of hydrochar but also contribute to higher adsorption performance due to increased surface area and chemical reactivity (Cavali et al., 2023). Therefore, selecting appropriate lignocellulosic biomass is crucial in tailoring hydrochar properties for specific environmental applications, such as the removal of anionic dyes like Congo red (Abudi et al., 2025).

Several previous studies have demonstrated the potential of biomass-derived hydrochars as efficient adsorbents for dye and pollutant removal from wastewater. For instance, a novel protonated amino-modified bamboo hydrochar (PAHC) was synthesized via Aza-Michael addition, resulting in exceptional adsorption capacities for methyl orange and Cr(VI) (515.35 and 523.57 mg/g, respectively), primarily due to electrostatic interaction from grafted protonated amines (Chen et al., 2023). Another study investigated hydrochar prepared from sewage sludge and garden waste, showing that the presence of lignin-rich green waste enhanced adsorption of methylene blue (52.39 mg/g) through improved surface functionality and electrostatic interactions in alkaline conditions (Wu et al., 2024). Similarly, activated hydrochar (AHC) synthesized from sugarcane bagasse using phosphoric acid and NaOH demonstrated a high adsorption capacity of 357.14 mg/g for methylene blue, attributed to electrostatic attraction, hydrogen bonding, and ϕ–ϕ interactions, as well as intra-particle diffusion mechanisms (Zhou et al., 2022). Moreover, hydrochars derived from invasive Sosnowsky's hogweed have also been explored, where KOH-activated materials exhibited effective adsorption of methylene blue (146 mg/g) and metal ions such as Cu^{2+} (18 mg/g) (Ansone-Bertina et al., 2024). Adawiyah et al. (2024) synthesized hydrochar from *Areca catechu* L. fruit for the adsorption of Congo red anionic dye. *Areca catechu* L. hydrochar increased adsorption capacity by up to twice that of untreated areca fruit. Plants such as fountain grass (*Pennisetum setaceum*), commonly referred to as horsetail reed, possess a lignocellulosic structure similar to agricultural biomass and hold significant potential as a precursor for activated carbon materials. Thus, this study aims to fill this gap by investigating the possibility of fountain grass-based hydrochar as an alternative adsorbent for dye-laden wastewater.

In this study, fountain grass (*Pennisetum setaceum*) was selected as the feedstock for hydrochar production. This species is an invasive weed that grows abundantly in marginal lands and remains largely underutilized (Da Re et al., 2020). Its lignocellulosic composition—comprising approximately 14.82–17.06% lignin, 33.94–37.37% cellulose, and 38.47–38.97% hemicellulose—makes it an excellent candidate for producing carbon-rich materials through hydrothermal carbonization (Cabrera-García et al., 2023). The relatively high content of cellulose and hemicellulose favors carbon yield and porosity, while lignin contributes to surface reactivity and structural integrity. The utilization of fountain grass not only offers a low-cost and sustainable solution for dye removal but also supports biomass valorization and invasive species management. This research aims to evaluate the adsorption performance of fountain grass-derived hydrochar for the removal of Congo red from aqueous solution. The study includes the synthesis of hydrochar via hydrothermal methods with varying reaction times, characterization of its physicochemical properties, and assessment of its adsorption capacity under different conditions. The outcomes are expected to contribute to the development of environmentally friendly and locally sourced adsorbents for effective wastewater treatment.

2. EXPERIMENTAL SECTION

2.1 Chemicals

The materials used in this study included fountain grass (*Pennisetum setaceum*) obtained from Palembang, Indonesia, hydrochloric acid (HCl), sodium chloride (NaCl), sodium hydroxide (NaOH), both purchased from Sigma-Aldrich, distilled water, and commercial Congo red. None of the materials underwent a purification process.

2.2 Instruments

The instruments used in this study included characterization tools such as a Rigaku MiniFlex 600 X-Ray Diffractometer (XRD), a Shimadzu Prestige-21 Fourier Transform Infrared (FT-IR) spectrophotometer, a BELSORP-miniX Brunauer-Emmett-Teller (BET) analyzer, a Quanta 650 Scanning Electron Microscope Energy Dispersive Spectrometer (SEM-EDS), and an EMC-18PC-UV UV-Vis spectrophotometer.

2.3 Preparation of *Pennicetum setaceum* Hydrochar

Hydrochar preparation from *Pennisetum setaceum* was carried out based on a previously reported method (Adawiyah et al., 2024), with the addition of time variations. The

Pennisetum setaceum (PS) plant parts (flowers, leaves, and stems) were dried and pulverized. Subsequently, 2.5 g of PS powder was weighed and mixed with 50 mL of distilled water. The mixture was transferred into a hydrothermal reactor tube and heated in an oven at 250°C for varying durations of 1, 2, 3, and 4 hours. The resulting PS hydrochar (HPS-1, HPS-2, HPS-3, and HPS-4) was then dried and ground into a fine powder for further characterization.

2.4 pHpzc Determination

The determination of pH point of zero charge (pHpzc) aims to identify the surface charge characteristics of the adsorbent material. A 2 M NaCl solution (20 mL) is prepared, and its pH is adjusted in the range of 3 to 10. Subsequently, 20 mg of the adsorbent (PS, HPS-1, HPS-2, HPS-3, and HPS-4) is added to each solution and stirred for 24 hours. The final pH is then measured to calculate the ΔpH (pH final-pH initial), which is used to construct the pHpzc curve.

2.5 Adsorption Performance

2.5.1 Comparison of Adsorbent Performance

Congo red (CR) solution was prepared at a concentration of 30 mg/L (40 mL) and added to the adsorbent materials (PS, HPS-1, HPS-2, HPS-3, and HPS-4). The mixture was allowed to undergo adsorption for 2 hours. After the contact time, the final concentration was measured using UV-Vis spectroscopy to calculate the adsorption capacity (Q_e) based on Equation 1.

$$Q_e = \frac{(C_0 - C_e)\,V}{C_0\,m} \tag{1}$$

where C_0 and C_t are the initial and final concentrations (mg/L), respectively, V is the volume of the solution (L), and m is the mass of the adsorbent (g).

2.5.2 Effect of pH

A total of 40 mL of CR with a concentration of 40 mg/L was adjusted to a pH of 5-10. It was then adsorbed with 20 mg of adsorbent for 2 hours. The final concentration was measured, and the adsorption capacity was calculated using Equation 1.

2.5.3 Effect of Reaction Time

The effect of reaction time was investigated to evaluate the adsorption kinetics of the adsorbent. A 40 mL Congo red (CR) solution (50 mg/L) was contacted with 20 mg of adsorbent for varying reaction times ranging from 0 to 120 minutes at 10-minute intervals. The optimum time was determined when the adsorption capacity reached equilibrium (Q_e), and the kinetic behavior was analyzed using pseudo-first-order (Equation 2) and pseudo-second-order (Equation 3) models.

$$\log(Q_e - Q_t) = \log Q_e - \frac{k_1}{2.303}t \tag{2}$$

$$\frac{t}{Q_t} = \frac{1}{k_2 Q_e^2}t + \frac{1}{Q_e} \tag{3}$$

Here, Q_e represents the amount of dye adsorbed at equilibrium (mg/g), Q_t is the amount adsorbed at time t (mg/g), k_1 is the rate constant of the pseudo-first-order (PFO) adsorption (1/min), and t is the contact time (min), k_2 is the rate constant of the pseudo-second-order (PFO).

2.5.4 Effect of Initial Concentration and Temperature

The effects of CR concentration and reaction temperature were studied to determine the adsorption behavior of the material based on its isotherm and thermodynamics. The initial CR concentration was varied at 30, 40, and 50 mg/L, while the testing temperature was set at 30°C, 40°C, and 50°C. In each experiment, 20 mg of adsorbent was mixed into 40 mL of CR solution. The equilibrium data obtained under optimal pH and reaction time conditions were analyzed using the Langmuir isotherm model (Equation 4) and the Freundlich isotherm model (Equation 5).

$$\frac{1}{Q_e} = \frac{1}{Q_{\max}} + \frac{1}{K_L Q_{\max} C_e} \tag{4}$$

$$\log Q_e = \log K_F + \frac{1}{n}\log C_e \tag{5}$$

The Q_{max} parameter describes the maximum adsorption capacity (mg/g), Ce is the concentration of the solution at equilibrium (mg/L), while K_L indicates the Langmuir constant, which represents the affinity between the adsorbent and the adsorbate. In the Freundlich model, K_F is related to adsorption capacity, and n describes the intensity and degree of heterogeneity of the adsorbent surface.

To evaluate the thermodynamic aspects of the adsorption process, experiments were conducted at several different temperatures. Changes in standard Gibbs free energy (ΔG°) were calculated using the relationship between the distribution coefficient (K_d), gas constant (R), and temperature (T) (Equation 6). Subsequently, the values of enthalpy change (ΔH°) and entropy change (ΔS°) were obtained from the $\ln K_d$ versus $1/T$ graph using a linear equation approach (Equation 7).

$$\Delta G^\circ = -RT \ln K_d \tag{6}$$

$$\ln K_d = \frac{\Delta S^\circ}{R} - \frac{\Delta H^\circ}{RT} \tag{7}$$

2.5.5 Regeneration

The regeneration treatment was aimed at studying the stability of the adsorbent structure. 40 mL of Cr (50 mg/L) was adsorbed with 20 mg of adsorbent at the optimum time. The final concentration was measured, and the efficiency value was calculated (Equation 8). The adsorbent was then separated from the adsorbate and ultrasonicated for 20 minutes for reuse up to three regeneration cycles.

$$\%\,\text{Efficiency} = \frac{C_0 - C_t}{C_0} \times 100\% \quad (8)$$

3. RESULTS AND DISCUSSION

3.1 Characterization of Materials

3.1.1 FT-IR Analysis

Based on the FTIR spectra (Figure 1a), all samples showed typical absorption bands of lignocellulosic materials. The broad absorption bands at 3200-3500 cm^{-1} indicate the presence of hydroxyl groups (−OH) (Amado-Fierro et al., 2025). The band at 3000-2800 cm^{-1} reflects the stretching of C−H aliphatic groups (Guo et al., 2025), while the bands around 1735 cm^{-1} and 1640 cm^{-1} indicate the presence of carbonyl groups (C=O) and C=C bonds of the aromatic structure of lignin, respectively (Kousar et al., 2025; Zhang et al., 2025). The absorption bands at 1113 and 1037 cm^{-1} correspond to ether (C−O−C) and methoxy (C−O) groups (Daer et al., 2024). The intensity of these bands decreased from HPS-1 to HPS-4, indicating the progressive degradation of functional groups due to the longer hydrothermal process (1-4 hours) at a fixed temperature of 250°C. This decrease indicates that longer reaction times result in the release of polar groups such as hydroxyl and carbonyl, thus impacting the surface composition of the adsorbent material.

3.1.2 XRD Analysis

The XRD diffractograms in Figure 1b show the changes in crystalline structure from the starting material (PS) to various hydrochar products (HPS-1 to HPS-4) after hydrothermal treatment. The PS sample shows a wide and irregular diffraction pattern, indicating the amorphous nature of the initial biomass. After hydrothermal treatment, the diffraction patterns underwent significant changes, particularly in HPS-1 and HPS-2, which exhibited sharper diffraction peaks at $2\theta = 15°$ and 22°. These peaks correspond to the (002) planes of cellulose-derived carbon (Le et al., 2025; Li et al., 2025), indicating an increase in structural regularity due to the formation of small-sized aromatic domains or reorientation of some functional groups into semi-crystalline structures. However, in HPS-3 and HPS-4, the intensity of these peaks began to decrease and become broader, indicating the hydrothermal process causes decomposition of the crystalline structure of cellulose and produces hydrochar dominated by amorphous structures, such as lignin, similar to the results reported in other biomass after hydrothermal treatment (Li et al., 2020; Pasipanodya et al., 2025; Zhao et al., 2025). These results indicate that hydrothermal treatment not only affects the microcrystalline structure of biomass but also plays a crucial role in determining the surface properties and porosity of hydrochar materials, which in turn influence their applications in adsorption.

3.1.3 Morphology Analysis

The SEM analysis results in Figures 2a–e show changes in the surface morphology of the raw material (PS) and hydrochar (HPS-1 to HPS-4) after hydrothermal treatment at 250°C with varying reaction times. The PS sample (Figure 2 relatively smooth surface with intact fiber structure, indicating the characteristics of the original biomass. After a 1-hour hydrothermal process (HPS-1, Figure 2 surface begins to crack, and small fragments form, indicating the onset of lignocellulose structure degradation. In HPS-2 and HPS-3 (Figures 2–d), the surface appears increasingly irregular with smaller particles and indications of pore formation. HPS-4 (Figure 2) exhibits a more porous morphology and rougher surface compared to other samples, indicating a higher degree of biomass decomposition.

The particle size distribution in the inset of each image shows the dominance of particles smaller than 10 μm in all hydrochar samples, which has the potential to increase the specific surface area and provide more active sites on the material. The EDS results (Table 1) confirm the change in elemental composition due to hydrothermal treatment. The carbon content increased from 62.85% (atomic 70.99%) in PS to 77.60% (atomic 82.67%) in HPS-4, while the oxygen content decreased from 31.11% to 20.68%. This trend indicates deoxygenation through the release of oxygen functional groups, likely due to dehydration and decarboxylation reactions during treatment (Xu et al., 2022). The content of mineral elements (Al and Si) also relatively decreased, indicating a reduction in inorganic impurities. The morphological changes accompanied by increased carbon content indicate that hydrothermal treatment not only improves surface texture but also modifies chemical composition (Chen et al., 2024; Prasannamedha et al., 2025; Saha et al., 2020), both of which play important roles in enhancing the adsorption properties of hydrochar.

3.1.4 Surface Area Analysis

The N_2 adsorption-desorption isotherm of the HPS-4 sample is shown in Figure 3 The isotherm curve shows a pattern resembling type IV with slight hysteresis at relatively high pressures $P/P_0 > 0.8$), indicating the presence of mesopores (Shanavas Laila and M. Sambasivam, 2025). BT analysis showed a specific surface area of 9.316 m^2/g with a total pore volume of 0.01092 cm^3/g. The average pore diameter obtained was 1.912 nm, which is in the micropore range (< 2 nm) according to the IUPAC classification (Gao et al., 2025)

Table 1. Materials Composition

Materials	Element (%)				Atomic (%)			
	C	O	Al	Si	C	O	Al	Si
PS	62.85	31.11	2.78	0.60	70.99	26.38	1.40	0.29
HPS-1	64.24	34.32	0.90	0.54	70.88	28.43	0.44	0.25
HPS-2	71.91	27.48	0.25	0.37	77.48	22.23	0.12	0.17
HPS-3	72.00	17.60	0.21	0.54	80.62	14.79	0.09	0.26
HPS-4	77.60	20.68	0.78	0.69	82.67	16.54	0.37	0.31

Table 2. PFO and PSO Parameters of HPS-4

Adsorbent	Qe Exp (mg/L)	PFO			PSO		
		Qe Calc (mg/L)	k_1	R^2	Qe Calc (mg/L)	k_2	R^2
HPS-4	34.070 ± 1.912	34.836 ± 0.899	0.031 ± 0.002	0.986	45.298 ± 2.770	6.238E-4 ± 1.472E-4	0.973

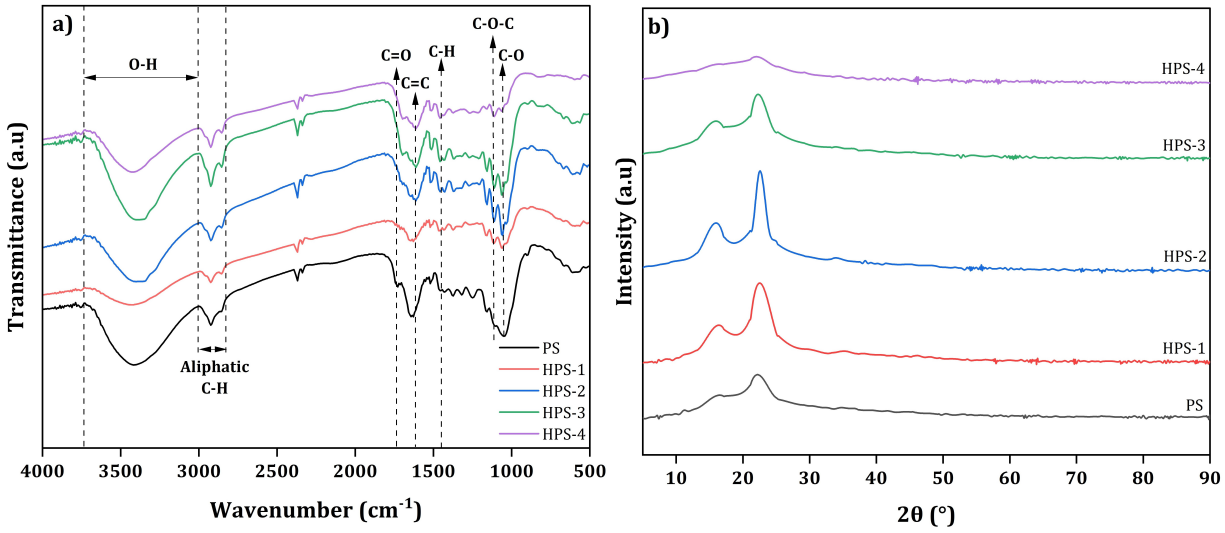

Figure 1. FTIR Spectra a) and XRD Diffractograms b) of PS, HPS-1, HPS-2, HPS-3, and HPS-4

This value indicates that the hydrothermal process with a longer reaction time contributes to pore formation and improved surface characteristics (Prasannamedha et al., 2025). This is also in line with the SEM results Figure 2e, where the surface of HPS-4 looks rougher and more porous, and is supported by EDS analysis (Table 1) shows an increase in carbon content due to dehydration and decarboxylation reactions. The combination of micropores and mesopores in HPS-4 offers improved active site accessibility, thereby enhancing the adsorption performance towards organic pollutants.

3.2 pHpzc Determination

pHpzc is the pH at which the surface of an adsorbent material is neutral, i.e., the positive and negative charges on its surface are balanced (Boucherdoud et al., 2025). The pHpzc values of PS material and its hydrothermal products (HPS-1 to HPS-4) are shown in Figure 4a. The pHpzc values were obtained from the intersection of the ΔpH curve with the initial pH horizontal line. The results show that the pHpzc for PS is 6.93, while for HPS-1, HPS-2, HPS-3, and HPS-4, the values are 7.22, 6.99, 6.06, and 5.44, respectively. It is evident that as the hydrothermal reaction time increases, the pHpzc value tends to decrease.

The differences in pHpzc values between samples indicate that the hydrothermal process affects the surface properties of the material. The longer the hydrothermal reaction time, the more the pHpzc tends to decrease, indicating that the surface becomes more acidic. This may be due to an increase in the number of oxygen functional groups or the degradation of organic structures during the hydrothermal process (Saha et al., 2019). The pHpzc value is important for determining which species are more easily adsorbed. At solution pH

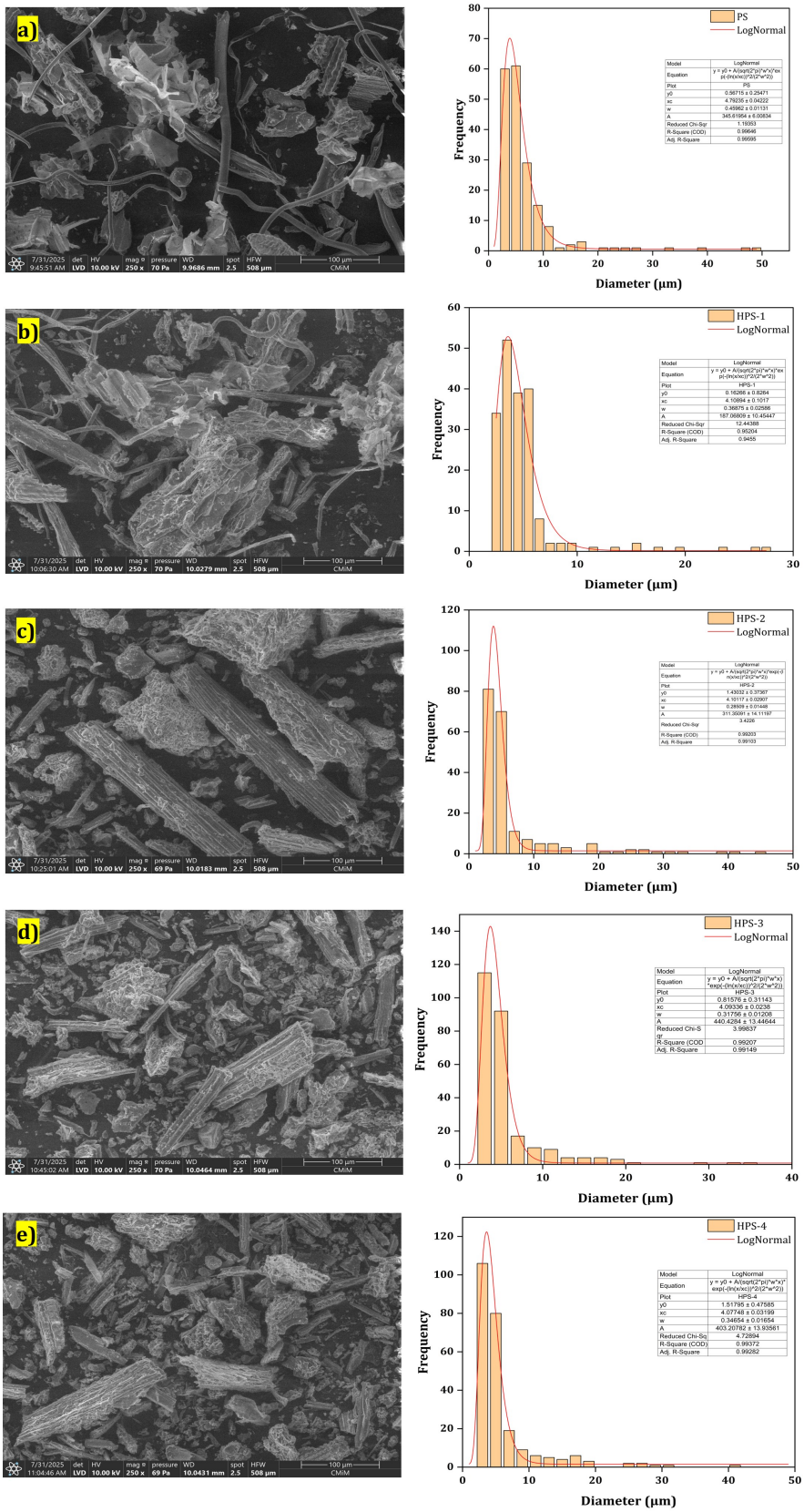

Figure 2. SEM Images and Histogram of a) PS, b) HPS-1, c) HPS-2, d) HPS-3, and e) HPS-4

Table 3. Adsorption Isotherms of HPS-4

Material	T (°C)	Langmuir			Freundlich		
		Q_{max}	K_L	R^2	N	K_F	R^2
HPS-4	40	51.67±5.46	2.211±8.21	0.98	54.87±452.08	51.15±19.89	0.01

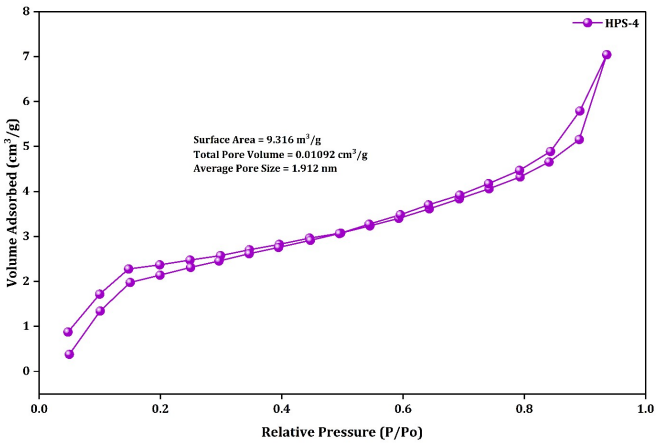

Figure 3. N_2 Adsorption-Desorption of HPS-4

below pHpzc, the adsorbent surface is positively charged, making it more effective at attracting anions, whereas at pH above pHpzc, the surface is negatively charged and more suitable for cation adsorption (Ewis et al., 2022; Tcheka et al., 2024).

3.3 Adsorption Performance

3.3.1 Adsorbents Optimum

Figure 4b shows the adsorption capacity (Q_e) of Congo Red on PS and hydrochar resulting from hydrothermal treatment (HPS-1 to HPS-4). PS showed the lowest capacity of 2.815 mg/g, which increased significantly after hydrothermal treatment. Increasing the reaction time from 1 hour (HPS-1) to 4 hours (HPS-4) resulted in a consistent upward trend in Q_e, with values of 24.754, 26.359, 31.833, and 37.864 mg/g, respectively. This increase indicates that hydrothermal treatment can improve surface characteristics, such as increasing surface area, enhancing pore number, and maintaining active functional groups involved in electrostatic interactions and hydrogen bonding with CR molecules (Selvaraj et al., 2025). HPS-4 exhibits the highest adsorption capacity, likely due to a combination of a more developed pore structure and greater availability of active sites for adsorption.

3.3.2 Effect of pH

Figure 4c shows the effect of solution pH on the adsorption capacity (Q_e) of CR dye by HPS-4 adsorbent. It can be seen that the highest adsorption capacity was obtained at pH 5, which was about 38.277 mg/g. The Q_e value decreased gradually as the pH of the solution increased, with the lowest capacity of approximately 24.473 mg/g at pH 10. These results indicate that acidic conditions are more favorable to the adsorption efficiency of CR by HPS-4.

CR is an anionic dye containing negatively charged sulfonate groups (de Melo et al., 2025; Wan et al., 2025). At pH 5, the surface of HPS-4 is still positively charged because it is below the pHpzc value (5.44), so the electrostatic interaction between the adsorbent surface and CR molecules becomes stronger (Ewis et al., 2022; Tcheka et al., 2024). As the pH increases, the surface of HPS-4 becomes negatively charged, causing repulsive forces with CR molecules, which results in a decrease in adsorption capacity. Therefore, pH 5 was determined as the optimum condition for CR adsorption by HPS-4, as it resulted in the most effective electrostatic interaction.

3.3.3 Effect of Reaction Time

Figure 4d shows the adsorption kinetics curve of CR by HPS-4 adsorbent, with the adsorbate concentration in solution decreasing with time until it reaches equilibrium. The adsorption capacity increased significantly during the first 60 minutes, then slowed down to equilibrium at around 100 minutes, which was determined as the optimum contact time.

Kinetics modeling was performed using the PFO and PSO models. Based on the parameters obtained in Table 2, the PFO model yielded more suitable results, with a theoretical Qe value of 34.836 ± 0.899 mg/g and an R^2 value of 0.986, which is in close agreement with the experimental Qe value of 34.070 ± 1.912 mg/g. Meanwhile, the PSO model showed a higher Qe value than the experiment, which was 45.298 ± 2.770 mg/g, with an R^2 of 0.973. These results indicate that the adsorption mechanism of CR by HPS-4 predominantly follows the PSO model, suggesting that the adsorption process occurs through physical interaction and that the adsorption rate depends on the concentration of the adsorbate remaining in the solution (Kloster et al., 2025; Shukla et al., 2025).

3.3.4 Effect of Initial Concentration and Temperature

Adsorption isotherm models were used to understand how CR dye molecules interact with the HPS-4 adsorbent surface. Two commonly used models are Langmuir and Freundlich. The Langmuir model assumes that adsorption occurs on a homogeneous surface with uniform active sites and forms only a monolayer, with no interactions between adsorbate molecules (Ahmia et al., 2026; Asif et al., 2025). In contrast,

Table 4. Adsorption Thermodynamics of HPS-4

Material	C (mg/L)	ΔH° (kJ/mol)	ΔS° (kJ/mol·K)	ΔG° (kJ/mol)		
				303 K	313 K	323 K
HPS-4	40	-44.070 ± 1.423	-0.129 ± 0.046	-4.980 ± 1.993	-3.690 ± 2.026	-2.400 ± 2.061

Table 5. Comparison of CR Adsorption

Adsorbent	Time (minutes)	Kinetics	Isotherms	Q_{max} (mg/g)	References
Pomegranate Peel Waste-Activated Carbon	240	PSO and Elovich	Langmuir	26.930	(Benahdach et al., 2025)
Cu/Al-LDHs@Gelatin	35	PSO	Jovanovic	10.354	(Nabil et al., 2025)
Chitosan@MnFe2O4 MNPs	30	PSO	Freundlich	40.800	(Khan et al., 2025)
Tetraethylenepentamine-Peanut Husks	200	PSO	Freundlich	19.569	(Chan et al., 2024)
Ni MOF Nanosheet-Infused CA-Modified PEI Membrane	300	PFO	Langmuir	23.300	(Kannivelan and Rajappan, 2025)
MIL-101(Fe)-Pyr	120	PSO	Freundlich	47.850	(Zauška et al., 2025)
Reduced Graphitic Oxide	240	PSO	Temkin and Freundlich	41.33	(Seemab et al., 2025)
Hydroxyapatite (HAp)	60	PSO	Langmuir	9.640	(Bin Mobarak et al., 2023)
A. *catechu* Hydrochar	180	PSO	Freundlich	40.515	(Adawiyah et al., 2024)
HPS-4	100	PFO	Langmuir	51.546	This Research

the Freundlich model describes adsorption on heterogeneous surfaces with non-uniform adsorption energies and allows the formation of multilayers (Alqarni et al., 2025; Deivayanai et al., 2025). Therefore, matching the experimental data with each model can provide insight into the nature of the adsorbent surface and the dominant adsorption mechanism.

Based on the analysis results at 40°C, the adsorption data of CR by HPS-4 is more in line with the Langmuir model, as indicated by the R^2 value of 0.988 (Table 3). The maximum adsorption capacity (Q_{max}) value reached 51.674 ± 5.468 mg/g, and the Langmuir affinity constant (K_L) was 2.211 ± 8.211, indicating a good affinity between CR and the adsorbent surface. In contrast, the Freundlich model yielded a very low R^2 value of 0.014, with an n value of 54.874 ± 452.080 and K_F of 51.154 ± 19.890, indicating that this model is not suitable for describing this adsorption system. Thus, it can be concluded that the adsorption of CR by HPS-4 takes place in a monolayer on a relatively homogeneous surface.

Thermodynamic studies were conducted to understand the energy properties of the CR adsorption process by HPS-4, through the calculation of standard enthalpy change (ΔH°), standard entropy (ΔS°), and standard Gibbs free energy (ΔG°) parameters at three different temperatures (303, 313, and 323 K) (Table 4). The ΔH° value obtained was -44.070 ± 1.423 kJ/mol, indicating that the adsorption process was exothermic (Su et al., 2025). Meanwhile, the ΔS° value was negative at -0.129 ± 0.046 kJ/mol · K, indicating a decrease in system order at the adsorbent-adsorbate interface during the process (Suebphanpho et al., 2025).

The negative ΔG° values at all three temperatures, namely -4.980 ± 1.993 kJ/mol (303 K), -3.690 ± 2.026 kJ/mol (313 K), and -2.400 ± 2.061 kJ/mol (323 K), indicate that the adsorption of CR by HPS-4 is spontaneous under the conditions studied (Yu et al., 2025). However, the tendency of ΔG° values to become smaller (less negative) as temperature increases suggests that increasing temperature reduces the spontaneity of the process, which is consistent with its exothermic nature. When the kinetic, isotherm, and thermodynamic results are considered together, the adsorption of CR by HPS-4 can be classified as a physico-chemical adsorption process. This is supported by the predominance of the PFO model (physisorption tendency), the conformity with the Langmuir isotherm (monolayer adsorption), and the ΔH° value lying in the transition range between physisorption and chemisorption. Furthermore, as shown in Table 4, HPS-4 exhibits a competitive maximum adsorption capacity compared to various other adsorbents reported in the literature, highlighting its strong potential for practical dye removal applications.

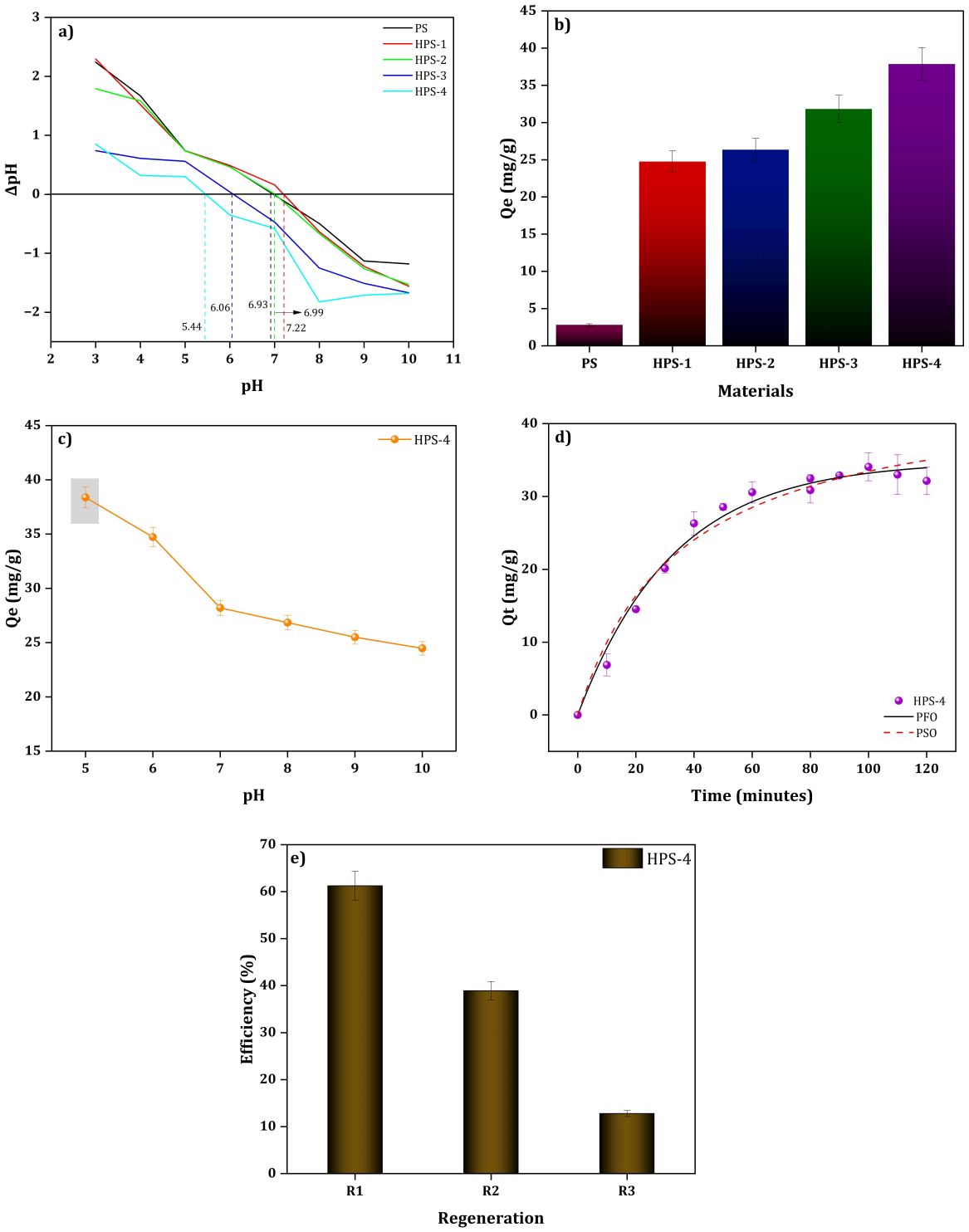

Figure 4. pHpzc Determination, b) Adsorbent Optimum, c) Effect of pH, d) Kinetics Adsorption, e) Regenerations

3.3.5 Regeneration Study

Regeneration ability is a crucial factor in evaluating the sustainability and efficiency of adsorbent reuse (Asif et al., 2025; Marouani et al., 2025). In this study, regeneration was performed on HPS-4 for three cycles to evaluate the stability of adsorption performance for CR (Figure 4e). The results are shown in Figure 4e, which shows that the adsorption efficiency decreased significantly as the number of cycles

increased. In the first cycle (R1), HPS-4 showed an efficiency of 61.26%, but decreased to 38.91% in the second cycle (R2), and only 12.78% in the third cycle (R3). This decrease in efficiency can be caused by loss of active groups, changes in surface structure, or blockage of pores by dye molecules that are not completely desorbed (Baaloudj et al., 2025; Yang et al., 2025). In addition, the regeneration treatment may also cause degradation of the adsorbent structure, which contributes to the decrease in performance. These results indicate that although HPS-4 has a high initial efficiency, its use as a regenerative adsorbent is still limited and needs further development.

3.3.6 Mechanism of Congo Red Adsorption

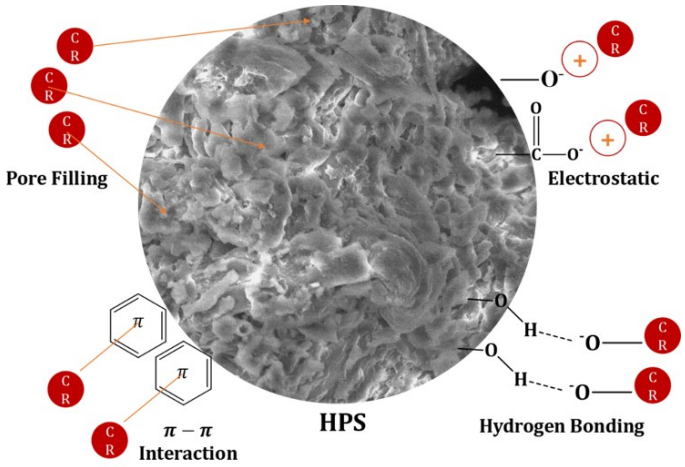

Figure 5. Adsorption Mechanism of CR by HPS

The adsorption mechanism (Figure 5) shows that CR molecules are distributed around and enter the pores of the HPS-4 hydrochar surface. Based on the adsorption results, HPS-4 has the highest capacity (37.87 mg/g) compared to other samples, indicating greater pore availability and more even distribution of active sites. The surface of HPS-4, as identified from SEM results, exhibits an open porous morphology, facilitating the diffusion of CR into the structure. The functional groups O–H, C=O, and C–O detected via FTIR play a crucial role in hydrogen bonding and electrostatic interactions with CR sulfonate groups, while the aromatic structure of biochar enables π–π stacking interactions with CR aromatic rings. Isotherm results following the Langmuir model indicate the formation of a monolayer on a homogeneous surface, while thermodynamic parameters (negative ΔG°) and kinetic compatibility with the PFO model suggest a combined mechanism of physisorption and chemisorption. The combination of morphological properties, surface chemistry, and pore structure explains the high adsorption performance of HPS-4 toward CR.

4. CONCLUSIONS

Hydrochar derived from *Pennisetum setaceum* through hydrothermal treatment exhibited a significant increase in CR adsorption capacity as the reaction time increased from 1 to 4 hours. Among the samples, HPS-4 showed the highest performance, achieving a maximum adsorption capacity of 51.674 ± 5.468 mg/g under optimal conditions (pH 5 and a contact time of 100 min). The kinetic data were well described by the PFO model, while the isotherm data followed the Langmuir model, suggesting the formation of a monolayer on a homogeneous surface. Thermodynamic analysis indicated that the adsorption process was spontaneous and exothermic, with $\Delta H^\circ = -44.07$ kJ/mol, $\Delta S^\circ = -0.129$ kJ/mol·K, and ΔG° values of -4.980, -3.690, and -2.400 kJ/mol at 303, 313, and 323 K, respectively. FTIR characterization confirmed the presence of functional groups O–H, C=O, C–O–C, and C–O, which are responsible for hydrogen bonding and electrostatic interactions with CR molecules. XRD analysis revealed an amorphous structure, supporting the availability of active sites. SEM–EDS showed a porous morphology with high carbon content and reduced oxygen content due to deoxygenation. BET analysis of HPS-4 further supported these findings, with a surface area of 2.166 m^2/g and an average pore diameter of 1.912 nm, indicating a predominantly microporous structure with limited mesoporosity, which correlates with the observed adsorption behavior. The adsorption mechanism is proposed to involve a combination of physisorption and chemisorption through electrostatic interactions, hydrogen bonding, and π–π stacking. However, regeneration studies demonstrated a significant decrease in performance after three cycles, highlighting limitations in reusability and stability.

Acknowledgement

We gratefully acknowledge the Research Center of Inorganic Materials and Complexes, Universitas Sriwijaya, for their invaluable support and contributions to the successful completion of this study.

REFERENCES

Abudi, Z. N., R. Al-Saedi, and A. R. Abood (2025). Adsorptive Uptake of Acetaminophen by Agricultural Waste-Derived Hydrochar: Kinetics, Isotherms, and Characterization Studies. *Sustainability (Switzerland)*, **17**(5); 2071–1050

Adawiyah, R., N. Yuliasari, Y. Hanifah, K. Alawiyah, and N. Rahayu Palapa (2024). Utilizing *Areca catechu* L. Fruit Peel-Derived Biochar and Hydrochar for Congo Red Adsorption: Kinetic and Thermodynamic Analysis. *Indonesian Journal of Environmental Management and Sustainability*, **8**(4); 135–144

Ahmad, N., A. R. Marlan, and S. P. J. Negara (2024). Insight of Anionic Dyes Adsorption from Their Aqueous Solutions onto MgAl LDH/Lignin: Characterization and Isotherm

Studies. *Indonesian Journal of Material Research*, **2**(2); 40–46

Ahmad, N., F. Suryani Arsyad, I. Royani, P. Mega Syah Bahar Nur Siregar, T. Taher, and A. Lesbani (2023). High Regeneration of ZnAl/NiAl-Magnetite Humic Acid for Adsorption of Congo Red from Aqueous Solution. *Inorganic Chemistry Communications*, **150**; 110517

Ahmed, H. M., M. E. Fawzy, and H. F. Nassar (2022). Effective Chemical Coagulation Treatment Process for Cationic and Anionic Dyes Degradation. *Egyptian Journal of Chemistry*, **65**(8); 301–310

Ahmia, N., M. Benamira, L. Messaadia, R. Masmoudi, D. Horwat, and I. Avramova (2026). Sol-Gel Auto-Combustion Synthesized $ZnMn_2O_4$ for Efficient Photocatalytic Congo Red Degradation: Structural, Kinetics, Computational, and Ecotoxicity Analyses. *Journal of Physics and Chemistry of Solids*, **208**; 113038

Akhtar, M. S., S. Ali, and W. Zaman (2024). Innovative Adsorbents for Pollutant Removal: Exploring the Latest Research and Applications. *Molecules*, **29**(18); 4317

Alegbe, E. O. and T. O. Uthman (2024). A Review of History, Properties, Classification, Applications and Challenges of Natural and Synthetic Dyes. *Heliyon*, **10**(13); e33646

Alqarni, L. S., M. N. Goda, M. Q. Alfaifi, M. Aleid, A. H. Ahmed, A. Alsulami, and A. Modwi (2025). Congo Red Eradication via Efficient La-NiO-g-C_3N_4 Nanocomposite from Contaminated Water. *Journal of Hazardous Materials Advances*, **18**; 100751

Amado-Fierro, Á., T. Offermans, J. Jansen, T. A. Centeno, and M. A. Díez (2025). Chemometrics to Connect Feedstock Quality, Process Settings and Calorific Value of Hydrochar Through Infrared Spectra. *Fuel Processing Technology*, **271**; 108201

Ansone-Bertina, L., L. Arbidans, E. Borska, U. Ozola, O. Purmalis, K. Sarsuns, L. Dobkevica, A. Sarakovskis, M. Klavins, and L. Klavins (2024). Modification and Activation of Hydrochar Obtained by the Hydrothermal Carbonisation Process of Invasive Plant Biomass. *Bioresource Technology Reports*, **26**; 101863

Asif, F. R., B. Bibi, M. Yasir, I. A. Khan, J. Gul, M. Irfan, S. Javed, and V. Sedlarik (2025). Polyester Waste Activated Carbon Assisted Micropollutant Methylene Blue and Congo Red Dyes Removal from Wastewater: RSM Modeling, Kinetics, Mechanism, and Reusability Study. *Journal of Industrial and Engineering Chemistry*

Baaloudj, O., F. Langerame, R. Iunnissi, G. Buttiglieri, D. Del Buono, S. Khadhar, L. Scrano, V. Trotta, and M. Brienza (2025). Biochar-Based Downflow Fixed-Bed Adsorption Systems for Water Treatment: Process Optimization, Reusability, and Techno-Economic Evaluation. *Separation and Purification Technology*, **377**; 134347

Badaruddin, M., N. Ahmad, E. S. Fitri, A. Lesbani, and R. Mohadi (2022). Hydrochar and Humic Acid as Template of ZnAl Layered Double Hydroxide for Adsorption of Phenol. *Science and Technology Indonesia*, **7**(4); 492–499

Badran, A. M., U. Utra, N. S. Yussof, and M. J. K. Bashir (2023). Advancements in Adsorption Techniques for Sustainable Water Purification: A Focus on Lead Removal. *Separations*, **10**(11); 565

Benahdach, K., Y. Aoulad El Hadj Ali, A. Azzouz, M. d. Mar Cerrillo González, A. Chraka, R. El Mail, A. El Laghdach, A. Wahby, and B. Arhoun (2025). Synthesis of Activated Carbon by Microwave-Assisted Sulfuric Acid Activation for the Adsorption of Congo Red in Aqueous Medium: Kinetic, Isotherm, Thermodynamic, Molecular Dynamic, and Functional Theory Studies. *Journal of Molecular Liquids*, **420**; 126821

Bessaha, F., G. Bessaha, S. Ziane, and A. Khelifa (2023). Adsorption of Methyl Orange on Bentonite: Design, Modeling, and Analysis of Experiments. *Iranian Journal of Chemistry and Chemical Engineering*, **42**(10); 3306–3323

Bezerra, B. G. P., L. Bieseki, D. R. da Silva, and S. B. C. Pergher (2019). Development of a Zeolite A/LDH Composite for Simultaneous Cation and Anion Removal. *Materials*, **12**; 661

Bin Mobarak, M., N. S. Pinky, F. Chowdhury, M. S. Hossain, M. Mahmud, M. S. Quddus, S. A. Jahan, and S. Ahmed (2023). Environmental Remediation by Hydroxyapatite: Solid State Synthesis Utilizing Waste Chicken Eggshell and Adsorption Experiment with Congo Red Dye. *Journal of Saudi Chemical Society*, **27**(5); 101690

Boucherdoud, A., A. Seghier, D. E. Kherroub, O. Douinat, K. Dahmani, B. Bestani, and N. Benderdouche (2025). Autogenous Deposition of Copper Oxide onto Polyaniline Nanocomposite Catalysts for the Photodegradation of Methylene Blue and Congo Red: Experimental Inquiry, RSM Optimization, and DFT Calculation. *Materials Science and Engineering: B*, **314**; 118015

Cabrera-García, P., M. D. Marrero, A. N. Benítez, and R. Paz (2023). Valorization of *Pennisetum setaceum*: from Invasive Plant to Fiber Reinforcement of Injected Composites. *Plants*, **12**(9); 1777

Cavali, M., N. Libardi Junior, J. D. de Sena, A. L. Woiciechowski, C. R. Soccol, P. Belli Filho, R. Bayard, H. Benbelkacem, and A. B. de Castilhos Junior (2023). A Review on Hydrothermal Carbonization of Potential Biomass Wastes, Characterization and Environmental Applications of Hydrochar, and Biorefinery Perspectives of the Process. *Science of The Total Environment*, **857**; 159627

Chan, K. T., S. T. Ong, and S. T. Ha (2024). Adsorptive Removal of Congo Red Dye from Its Aqueous Solutions by Tetraethylenepentamine Modified Peanut Husks Composite Beads. *Desalination and Water Treatment*, **317**; 100060

Chen, S., B. Han, X. Chen, F. Xu, and G. Wang (2024). Hydrothermal Synthesis and Morphology Control Mechanism of $BaTiO_3$ from $NaTi_3O_6(OH)(H_2O)_2$ Precursors. *Ceramics International*, **50**(12); 21779–21787

Chen, Z. L., H. Xu, L. Q. Bai, Y. L. Feng, and B. Li (2023).

Protonated-Amino-Functionalized Bamboo Hydrochar for Efficient Removal of Hexavalent Chromium and Methyl Orange. *Progress in Natural Science: Materials International*, **33**(4); 501–507

Cui, C., W. Qiao, D. Li, and L. J. Wang (2025). Dual Cross-Linked Magnetic Gelatin/Carboxymethyl Cellulose Cryogels for Enhanced Congo Red Adsorption: Experimental Studies and Machine Learning Modelling. *Journal of Colloid and Interface Science*, **678**; 619–635

Cui, D., B. Zhang, S. Wu, X. Xu, B. Liu, Q. Wang, X. Zhang, and J. Zhang (2024). From Sewage Sludge and Lignocellulose to Hydrochar by Co-Hydrothermal Carbonization: Mechanism and Combustion Characteristics. *Energy*, **305**; 132414

Da Re, D., E. Tordoni, F. De Pascalis, Z. Negrín-Pérez, J. M. Fernández-Palacios, J. R. Arévalo, D. Rocchini, F. M. Medina, R. Otto, E. Arlé, and G. Bacaro (2020). Invasive Fountain Grass (*Pennisetum setaceum* (Forssk.) Chiov.) Increases Its Potential Area of Distribution in Tenerife Island Under Future Climatic Scenarios. *Plant Ecology*, **221**(10); 867–882

da Silva, M. D. C. R., D. M. Druzian, L. F. W. Brum, C. dos Santos, G. Pavoski, D. C. R. Espinosa, Y. P. M. Ruiz, A. Galembeck, and W. L. da Silva (2024). Green Synthesis of ZrO_2/PdO-NPs for Photodegradation of Anionic Dyes: Photocatalytic Activity and Machine Learning Modelling. *Journal of Molecular Liquids*, **410**; 125581

Daer, D., L. Luo, Y. Shang, J. Wang, C. Wu, and Z. Liu (2024). Co-Hydrothermal Carbonization of Waste Biomass and Phosphate Rock: Promoted Carbon Sequestration and Enhanced Phosphorus Bioavailability. *Biochar*, **6**(1); 70

de Melo, A. N., W. K. L. da Silva, C. C. da Silva, M. C. Ferreira, B. S. Damasceno, and A. C. V. de Araújo (2025). Magnetic Graphite Nanocomposite for the Removal of Reactive Black 5 and Congo Red from Textile Industry Wastewater. *Materials Chemistry and Physics*, **345**; 131230

Dehghani, M. H., S. Ahmadi, S. Ghosh, A. Othmani, C. Osagie, M. Meskini, S. S. AlKafaas, A. Malloum, W. A. Khanday, A. O. Jacob, Ö. Gökkuş, A. Oroke, O. Martins Chineme, R. R. Karri, and E. C. Lima (2023). Recent Advances on Sustainable Adsorbents for the Remediation of Noxious Pollutants from Water and Wastewater: A Critical Review. *Arabian Journal of Chemistry*, **16**(12); 105303

Dehingia, B., R. Lahkar, and H. Kalita (2024). Efficient Removal of Both Cationic and Anionic Dyes from Water Using a Single rGO/PSS Nanocomposite Membrane with Superior Permeability and High Aqueous Stability. *Journal of Environmental Chemical Engineering*, **12**(2); 112393

Deivayanai, V. C., S. Karishma, P. Thamarai, A. Saravanan, P. R. Yaashikaa, and A. S. Vickram (2025). Advanced Modeling of Congo Red Dye Adsorption Using Magnetic Nanoparticles Functionalized with Jackfruit Seed Waste Biomass: A Contemporary Modeling Approach. *Materials Chemistry and Physics*, **341**; 130947

Ewis, D., M. M. Ba-Abbad, A. Benamor, and M. H. El-Naas (2022). Adsorption of Organic Water Pollutants by Clays and Clay Minerals Composites: A Comprehensive Review. *Applied Clay Science*, **229**; 106686

Farjadfar, S., M. Ghiaci, S. A. Kulinch, and W. Wunderlich (2022). Efficient Photocatalyst for the Degradation of Cationic and Anionic Dyes Prepared via Modification of Carbonized Mesoporous TiO_2 by Encapsulation of Carbon Dots. *Materials Research Bulletin*, **155**; 111963

Fattahimoghaddam, H., T. Mahvelati-Shamsabadi, and B. K. Lee (2021). Efficient Photodegradation of Rhodamine B and Tetracycline over Robust and Green g-C_3N_4 Nanostructures: Supramolecular Design. *Journal of Hazardous Materials*, **403**; 123703

Gao, J., Z. Li, X. Tao, X. Li, and K. Zhu (2025). A Comprehensive Study of Multiscale Pore Structural Characteristics in Deep-Buried Coals of Different Ranks. *Scientific Reports*, **15**(1); 8299

Guo, W., Z. Zhang, B. Wang, L. Xue, and Y. Feng (2025). Novel Insights into Released Hydrochar Particle Derived from Typical High Nitrogen Waste Biomass: Special Properties, Microstructure and Formation Mechanism. *Waste Management*, **193**; 517–528

Güleç, F., L. M. G. Riesco, O. Williams, E. T. Kostas, A. Samson, and E. Lester (2021). Hydrothermal Conversion of Different Lignocellulosic Biomass Feedstocks – Effect of the Process Conditions on Hydrochar Structures. *Fuel*, **302**; 121166

He, J., L. Zhu, S. Guo, and B. Yang (2025). An Effective Strategy for Coal-Series Kaolin Utilization: Preparation of Magnetic Adsorbent for Congo Red Adsorption. *Chemical Engineering Science*, **304**; 120958

Jefri, J., N. A. Fithri, and A. Lesbani (2024). Enhanced Removal Efficiency of Malachite Green Dye Using Gambir Leaf Extract-Modified NiFe LDH Composites: A Study of Cationic Dye Adsorption. *Bulletin of Chemical Reaction Engineering & Catalysis*, **19**(4); 573–584

Jefri, J., N. A. Fithri, and N. Ramadhan (2025). Enhanced Selectivity of Ni/Al LDH for Cationic Dye Adsorption via Gambier Leaf Extract Modification. *Indonesian Journal of Material Research*, **3**(1); 1–7

Kannivelan, S. and K. Rajappan (2025). Design and Development of Ni MOF Nanosheet-Infused CA-Modified PEI Membrane for Enhanced Congo Red Adsorption. *Inorganic Chemistry Communications*, **178**; 114550

Kazak, O., G. K. Akkaya, and A. Tor (2023). Sustainable and Efficient Removal of Cationic, Anionic and Neutral Dyes from Water by Pre-Deposited Vinasse Biochar Membrane. *Journal of Environmental Chemical Engineering*, **11**(3); 110042

Khan, M. A., S. Kuldeep, Yadav, N. Singh, and G. A. Basheed (2025). Enhanced Adsorption of Congo Red Dye

Using Dried Chitosan Functionalized $MnFe_2O_4$ Viscoelastic Fluid. *Colloids and Surfaces A: Physicochemical and Engineering Aspects*, **709**; 136166

Khanzada, A. K., H. E. Al-Hazmi, T. A. Kurniawan, J. Majtacz, G. Piechota, G. Kumar, P. Ezzati, M. R. Saeb, N. Rabiee, H. Karimi-Maleh, E. C. Lima, and J. Makinia (2024). Hydrochar as a Bio-Based Adsorbent for Heavy Metals Removal: A Review of Production Processes, Adsorption Mechanisms, Kinetic Models, Regeneration and Reusability. *Science of The Total Environment*, **945**; 173972

Kloster, M., N. E. Marcovich, and M. A. Mosiewicki (2025). Microcrystalline Cellulose Modified Chitosan Aerogels To Enhance Congo Red Dye Adsorption. *Colloids and Surfaces A: Physicochemical and Engineering Aspects*, **707**; 135823

Kohzadi, S., N. Marzban, K. Godini, N. Amini, and A. Maleki (2023). Effect of Hydrochar Modification on the Adsorption of Methylene Blue From Aqueous Solution: An Experimental Study Followed by Intelligent Modeling. *Water*, **15**(18); 3220

Kousar, S., K. Javed, B. Begum, M. M. Naeem, S. Zhang, and X. Hu (2025). Organic Solvent Assisted Hydrothermal Processing of Cooked Rice To Get Insights Into the Evolution of Chemical Structure of Hydrochar. *Waste Management*, **205**; 115007

Kumari, U. (2024). Textile Dyes and Their Impact on the Natural Environment. In P. Singh, editor, *Dye Pollution From Textile Industry: Challenges and Opportunities for Sustainable Development*. Springer Nature Singapore, pages 17–30

Le, T. T. U., T. G. Ngo, N. A. Hoang, V. H. Nguyen, V. D. Nguyen, L. P. Hoang, T. D. Pham, and T. T. Truong (2025). Adsorption Characteristics of Single and Binary Mixture of Methylene Blue and Rhodamine B on Novel Hydrochar Derived From Lemongrass Essential Oil Distillation Residue. *Journal of Molecular Liquids*, **425**; 127205

Li, H. Z., Y. N. Zhang, J. Z. Guo, J. Q. Lv, W. W. Huan, and B. Li (2021). Preparation of Hydrochar With High Adsorption Performance for Methylene Blue by Co-Hydrothermal Carbonization of Polyvinyl Chloride and Bamboo. *Bioresource Technology*, **337**; 125442

Li, K., S. Yu, F. Han, C. Xu, Q. Li, Y. Zhang, and H. Zhou (2025). Decoupled Temperature and Pressure Strategies in Hydrothermal Process of Cellulose: A Comprehensive Study. *Fuel*, **381**; 133304

Li, Z., W. Yi, Z. Li, C. Tian, P. Fu, Y. Zhang, L. Zhou, and J. Teng (2020). Preparation of Solid Fuel Hydrochar Over Hydrothermal Carbonization of Red Jujube Branch. *Energies*, **13**(2); 480

Marouani, I., W. H. Hassan, N. S. S. Singh, M. Hasan, A. Abduvokhidov, M. Karimov, A. Abilkasimov, I. Mahariq, and M. A. Diab (2025). Preparation of a Novel Reusable 2D-MXene With Flower-Like LDH Composite for Ultra-High Adsorption of Congo Red and Doxycycline: Stability and Environmental Application. *Journal of Water Process Engineering*, **76**; 108288

Mohadi, R., N. Juleanti, N. Normah, P. M. S. B. N. Siregar, A. Wijaya, N. R. Palapa, and A. Lesbani (2022). Low-Cost Yet High-Performance Hydrochar Derived From Hydrothermal Carbonization of Duku Peel (*Lansium domesticum*) for Cr(VI) Removal From Aqueous Solution. *Indonesian Journal of Chemistry*, **22**(6); 1523–1533

Mortezapour, F., N. Shadjou, and M. Mahmoudian (2025). Effective Removal of Anionic Dyes From Aqueous Solution Using Polyethersulfone Based Membrane Reinforced by Montmorillonite. *BMC Chemistry*, **19**(1); 1–10

Munonde, T. S., N. Madima, R. Ratshiedana, P. Nosizo Nomngongo, L. E. Mofokeng, and R. S. Dima (2025). Synergistic Adsorption-Photocatalytic Remediation of Methylene Blue Dye From Textile Industry Wastewater Over NiFe LDH Supported on Tyre-Ash Derived Activated Carbon. *Applied Surface Science*, **679**; 161205

Nabil, G. M., R. H. Althomali, and M. E. Mahmoud (2025). Decorated Gelatin Polymer onto Copper Aluminum Layered Double Hydroxides for Superior Removal of Congo Red: Optimization and Adsorption Evaluation of Kinetics, Isotherms, and Thermodynamics. *Journal of Molecular Structure*, **1319**; 139303

Ojewumi, M. E. and G. Chen (2024). Hydrochar Production by Hydrothermal Carbonization: Microwave versus Supercritical Water Treatment. *Biomass*, **4**(2); 574–598

Pasipanodya, D., N. Seedat, B. Patel, and R. Roopchund (2025). Production of Hydrochar from the Hydrothermal Carbonisation of Food Waste Feedstock for Use as an Adsorbent in Removal of Heavy Metals from Water. *Biomass Conversion and Biorefinery*, **15**(8); 11819–11833

Phan, K. A., D. Phihusut, and N. Tuntiwiwattanapun (2022). Preparation of Rice Husk Hydrochar as an Atrazine Adsorbent: Optimization, Characterization, and Adsorption Mechanisms. *Journal of Environmental Chemical Engineering*, **10**(3); 107575

Prasannamedha, G., P. S. Kumar, S. R. Balasubramani, V. Parthasarathy, A. D. Deehen, E. Jananie, V. Lokesh, S. Shivani, S. Keerthana, I. Shivani, and G. Rangasamy (2025). Engineering Properties of Hydrochar Fabricated from Hydrothermal Carbonization of Lignocellulosic Biomass: Practice as Adsorbent and Catalyst in Water Treatment. *Journal of Water Process Engineering*, **74**; 107739

Rianjanu, A., T. Haloho, J. L. Pasaribu, A. G. Fahmi, E. Nurfani, W. S. Sipahutar, H. T. Yudistira, and T. Taher (2025). Electrospun Rare-Earth Metal Oxide (CeO_2) Nanofiber for the Degradation of Congo Red Aqueous Dyes. *Science and Technology Indonesia*, **10**(1); 123–130

Saha, N., K. McGaughy, and M. T. Reza (2020). Elucidating Hydrochar Morphology and Oxygen Functionality Change with Hydrothermal Treatment Temperature Ranging from Subcritical to Supercritical Conditions. *Journal*

of Analytical and Applied Pyrolysis, **152**; 104965

Saha, N., A. Saba, and M. T. Reza (2019). Effect of Hydrothermal Carbonization Temperature on pH, Dissociation Constants, and Acidic Functional Groups on Hydrochar from Cellulose and Wood. *Journal of Analytical and Applied Pyrolysis*, **137**; 138–145

Satyam, S. and S. Patra (2024). Innovations and Challenges in Adsorption-Based Wastewater Remediation: A Comprehensive Review. *Heliyon*, **10**(9); e29573

Seemab, S., S. Muhammad, S. Nawaz, S. Ahmad, R. Ullah, and A. Khan (2025). Exploring the Adsorption Potential of Waste Graphite Obtained from Spent Dry Cells for Congo Red Dye from Aqueous Solutions. *Chemical Engineering Science*, **306**; 121224

Selvaraj, P. S., P. Ettiyagounder, K. Sabarish, K. Periasamy, B. Rengasamy, D. Veeraswamy, T. Karchiyappan, and S. Kathirvel (2025). Hydrothermal Carbonization Approach for Transforming Biomass Waste to Value Added Hydrochar and Its Applications in Water Remediation. *Desalination and Water Treatment*, **322**; 101199

Shanavas Laila, L. and K. M. Sambasivam (2025). Enhancing the Efficiency of Mortar Mixes by Rice Husk Hydrochar Using Response Surface Methodology: An Experimental Study for Property Improvement and Sustainable Construction Applications. *Results in Engineering*, **27**; 106019

Shukla, A. K., J. Alam, and M. Alhoshan (2025). Trimesoyl Chloride Crosslinked Chitosan: An Efficient Adsorbent for Congo Red Dye Removal from Water - Kinetic and Isotherm Analysis. *International Journal of Biological Macromolecules*, **319**; 145538

Siddiqui, S. I., E. S. Allehyani, S. A. Al-Harbi, Z. Hasan, M. A. Abomuti, H. K. Rajor, and S. Oh (2023). Investigation of Congo Red Toxicity Towards Different Living Organisms: A Review. *Processes*, **11**(3); 807

Siregar, P. M. S. B. N., N. R. Palapa, A. Wijaya, E. S. Fitri, and A. Lesbani (2021). Structural Stability of Ni/Al Layered Double Hydroxide Supported on Graphite and Biochar Toward Adsorption of Congo Red. *Science and Technology Indonesia*, **6**(2); 85–95

Su, Y., Y. Wang, L. Ding, Y. Chen, and D. Song (2025). An Innovative and Efficient Strategy for Removing Congo Red Using Magnetic Hollow Zn/Co Zeolitic Imidazolate Framework Composite. *Environmental Research*, **264**; 120399

Suebphanpho, J., S. Chanchit, S. Phimphakan, and J. Boonmak (2025). Metallogel Synthesis from Cu(II) Complex with Benzotriazole-5-Carboxylic Acid for Enhanced Congo Red Dye Adsorption and Anion Exchange. *ACS Omega*

Tcheka, C., M. M. Conradie, V. A. Assinale, and J. Conradie (2024). Mesoporous Biochar Derived from Egyptian Doum Palm (Hyphaene Thebaica) Shells as Low-Cost and Biodegradable Adsorbent for the Removal of Methyl Orange Dye: Characterization, Kinetic and Adsorption Mechanism. *Chemical Physics Impact*, **8**; 100446

Tolkou, A. K., A. Giannoulaki, P. Chalkidi, E. Arvaniti, S. Fykari, S. Kritaki, and G. Z. Kyzas (2025). Removal of Anionic and Cationic Dyes from Wastewater by Tetravalent Tin-Based Novel Coagulants. *Processes*, **13**(7); 2103

Wan, H., X. Zhu, J. Wang, F. Cao, Y. Zhang, Z. Yao, S. Wang, D. Bhattacharyya, and K. Tang (2025). Adsorptive Nanofibrous Membranes for Bidirectional Removal of Cationic and Anionic Dyes. *Separation and Purification Technology*, **361**; 131515

Wei, Q., Y. Zhang, K. Zhang, J. I. Mwasiagi, X. Zhao, C. W. K. Chow, and R. Tang (2022). Removal of Direct Dyes by Coagulation: Adaptability and Mechanism Related to the Molecular Structure. *Korean Journal of Chemical Engineering*, **39**(7); 1850–1862

Wibiyan, S., I. Royani, and A. Lesbani (2024). Synthesis and Performance of ZnAl@Layered Double Hydroxide Composites with *Eucheuma cottonii* Adsorption and Regeneration of Congo Red Dye. *Indonesian Journal of Environmental Management and Sustainability*, **8**(3); 126–134

Wijaya, A. and N. Yuliasari (2023). Biochar Derived from Rice Husk as Effective Adsorbent for the Removal Congo Red and Procion Red MX-5B Dyes. *Indonesian Journal of Material Research*, **1**(1); 1–7

Wu, C., Z. Zhao, J. Zhong, Y. Lv, X. Yan, Y. Wu, and H. Zhang (2024). Adsorption of Dye Through Hydrochar Derived From Co-Hydrothermal Carbonization of Garden Waste and Sewage Sludge: The Adsorption Enhancement Mechanism of Lignin Component. *Journal of Water Process Engineering*, **67**; 106233

Xu, Z. X., X. Q. Ma, J. Zhou, P. G. Duan, W. Y. Zhou, A. Ahmad, and R. Luque (2022). The Influence of Key Reactions During Hydrothermal Carbonization of Sewage Sludge on Aqueous Phase Properties: A Review. *Journal of Analytical and Applied Pyrolysis*, **167**; 105678

Yang, H., G. Zhang, X. Chen, and W. Zhang (2025). Quaternized Fenugreek Gum Grafted Poly(Acrylamide-Co-Methacryloxyethyltrimethyl Ammonium Chloride) Novel Composite Hydrogel for Efficient Removal of Congo Red Dye. *International Journal of Biological Macromolecules*, **320**; 146090

You, H., B. Huang, C. Cao, X. Liu, X. Sun, L. Xiao, J. Qiu, Y. Luo, Q. Qian, and Q. Chen (2021). Adsorption–Desorption Behavior of Methylene Blue Onto Aged Polyethylene Microplastics in Aqueous Environments. *Marine Pollution Bulletin*, **167**; 112287

Yu, S., B. Peng, P. Wu, J. Li, Q. Liu, S. Li, Y. Gu, Y. Liu, Z. Lu, J. Wang, and J. Xing (2025). Deposition of Polydopamine Onto Magnetic Chitosan Microspheres for Efficient Adsorption of Congo Red and Easy Recycling. *Colloids and Surfaces A: Physicochemical and Engineering Aspects*, **722**; 137313

Zauška, Ł., P. Pillárová, D. Volavka, E. Kinnertová, J. Bednarčík, J. Brus, V. Hornebecq, and M. Almáši (2025). Kinetic Adsorption Mechanism of Cobalt(II) Ions and Congo Red on Pristine and Schiff Base-Surface-Modified MIL-101(Fe)-NH_2. *Microporous and Mesoporous Materi-*

als, **386**; 113493

Zhang, F., C. Liu, S. Wang, and Y. Zhang (2025). Fabricating Efficient SnO_2/Hydrochar Heterojunction Visible Light Photocatalyst for Cr(VI) Reduction. *Journal of Molecular Structure*, **1336**; 142084

Zhao, P., S. Yu, Y. S. Zhang, H. Cheng, X. Yang, Q. Li, Y. Zhang, and H. Zhou (2025). Ni Transformation and Hydrochar Properties During Hydrothermal Carbonization of Cellulose. *Fuel*, **382**; 133772

Zhou, F., K. Li, F. Hang, Z. Zhang, P. Chen, L. Wei, and C. Xie (2022). Efficient Removal of Methylene Blue by Activated Hydrochar Prepared by Hydrothermal Carbonization and NaOH Activation of Sugarcane Bagasse and Phosphoric Acid. *RSC Advances*, **12**(3); 1885–1896

